Force Controlled Laparoscopic Surgical Robot without Distal ForceSensing

Nabil Zemiti, Tobias Ortmaier, Marie-Aude Vitrani, Guillaume Morel

V. Medical Robotics

As robot applications in human environments increase, we see many interesting application in medicine. These include robotic technologies used in robot-doctor interfaces for minimally invasive surgery and novel robotic devices that can navigate inside human bodies. This chapter presents 3 interesting articles representing the various facets of medical robotics. Papers in other chapters, however, also describe medical applications of robotics.

The first article by Zemeti and co-workers presents the design and analysis of a Minimally Invasive Surgery robot. The trocar is designed with force measurement capability, where the force sensor is placed outside the patient – "to reduce cost and sterilizibility requirements". This paper presents the results of the feasibility experiments.

In the next article, Dario and colleagues take medical robotics a step further into the future by reporting on the concept and the preliminary modeling of legged micro robot locomoting in a tubular, slippery and compliant environment. The intended application is for the microrobots to navigate inside the gastrointestinal tract for diagnosis and therapy. The microcapsules are designed to be ingestible and then to make its way to the gastrointestinal tract. The new contribution being studied here is the micro robot's capability of effective locomotion while inside the human body.

The third article by Casals, *et al*. presents a multimodal approach to human-machine interface, applied to medical robotics. This carries a similar idea to the first article in Chapter XIII by Iba *et al*, under the heading of Haptics and Augmented Reality. The idea is to provide a range of media of communication between the surgeon and the robots, thus creating a quasi-hands-free control of the equipments. This would allow the surgeon to better control the equipments in the operating room without losing too much focus on the task at hand. The mode of interaction being studied is gesture recognition, with other modes available such as: tactile, speech, pedals, etc.

A Force Controlled Laparoscopic Surgical Robot without Distal Force Sensing

Nabil Zemiti, Tobias Ortmaier, Marie-Aude Vitrani, and Guillaume Morel

Laboratoire de Robotique de Paris (LRP), BP 61,
Route du Panorama, 92 265 Fontenay aux Roses Cedex, Paris, France

Abstract. Minimally invasive surgery (MIS) challenges the surgeon's skills due to his separation from the operation area which can be reached with long instruments only. Therefore, the surgeon loses access to the manipulation forces inside the patient. This reduces his dexterity when performing the operation. A new compact and lightweight robot for MIS is presented which allows for the measurement of manipulation forces. The main advantage of this concept is that no miniaturized force sensor has to be integrated into surgical instruments and inserted into the patient. Rather, a standard sensor is attached to a modified trocar outside the patient, which allows for the measurement of manipulation forces. This approach reduces costs and sterilizability demands. Results of first force control experiments are presented to show the feasibility of the concepts.

1 Introduction

The use of robots for surgical interventions is a an approach that is now proven to increase the quality of operations and to establish new types of surgical procedures (see [1] for an up-to-date overview of this research field). Especially, minimally invasive surgery (MIS) in which long instruments are used to gain access to the area of interest seems to be a promising field for robotic surgery. Here, robots help the surgeon to regain virtually direct access to the operation field he is seperated from: actuated instruments provide him with full dexterity inside the patient as in open surgery. In order to enhance the overall system performance, force control capabilities are desirable [2,3]. These forces can be used in two ways: it becomes possible to run the robot in a force controlled mode, helping to prevent unintentional damage of tissue or to compensate for organ motion in case of contact between instrument and organ [4]. Furthermore, manipulation forces can be displayed back to the surgeon (with appropriate kinesthetic input devices), providing him with direct sensation of the remote forces applied. Unfortunately, the therefore necessary measurement of manipulation forces in minimally invasive robotic surgery (MIRS) is rarely realized as appropriate small and sterilizable force sensors which can be inserted into the patient are still missing [5]. In this paper the new robot MC^2E (french abbreviation for compact manipulator for endoscopic surgery) is presented, offering a new possibility of force measurement in MIRS. The robot is shown in Fig. 1 during in vivo experiments realized at the Surgical School of Paris.

The reminder of this article is organized as follows: In Sect. 2 the robot's kinematics is presented. Section 3 describes the novel principle of force measurement

M.H. Ang and O. Khatib (Eds.): Experimental Robotics IX, STAR 21, pp. 153–163, 2006.

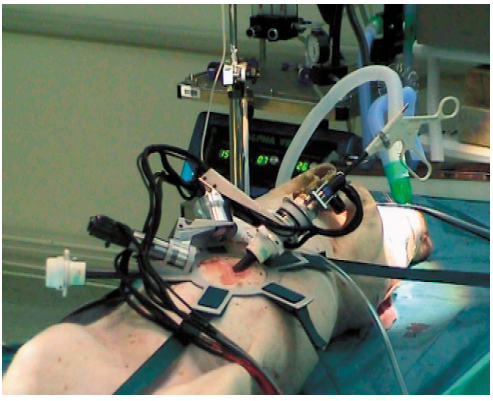

Fig. 1. MC^2E during in vivo experiments on a pig.

for MIRS in detail. Force control and experimental results are given in Sect. 4. A discussion of the results and further directions for research are given in Sect. 5.

2 Robot and Kinematics

A robot used in the operating room (OR) has to be lightweight and compact, as only a small amount of space for additional equippment is available. Furthermore, a lightweight robot can be easily mounted and removed by one nurse which helps to reduce preoperative setup time and is also a safety feature in emergency situations.

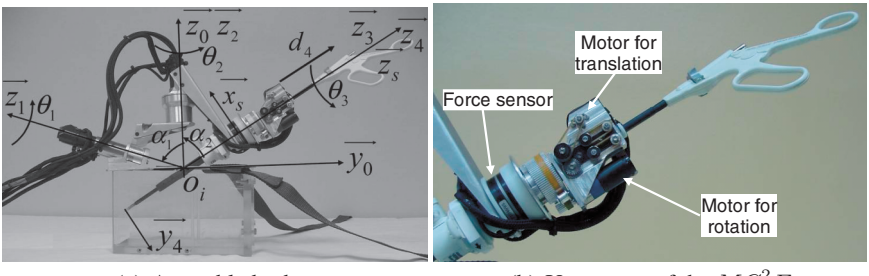

(a) Assembled robot (b) Upper part of the MC^2E

Fig. 2. MC^2E robot together with coordinate frames and Denavit-Hartenberg parameters.

Unlike most other MIS robots MC^2E moves not only the instrument but also the trocar in which the instrument is inserted. As shown in Fig. 2 the robot is comprised of two parts: the lower part moves the trocar and is a compact spherical 2 DoFs mechanism (Θ_1 and Θ_2) providing an invariant center at the fulcrum point. The base

of this lower subsystem is easily installed on the patient's body and clipped to the trocar. The upper part is mounted on the trocar and provides 2 DoFs: rotation about the instrument axis (Θ_3) and translation along the instrument axis (d_4). The upper part is depicted in detail in the right side of Fig. 2. The design of the robot is rather compact. Furthermore, it allows for the use of standard disposable instruments, and enables co-manipulation by the surgeon and the robot. Note that similar compact designs are proposed in [6,7].

Two different types of motors from *Faulhaber* were chosen: Two powerful motors (ref. 2342S024CR, 12 Watt) for the spherical part of the robot and two smaller motors (ref. 1724T003SR, 4 Watt) for the upper part of the robot. The encoder resolution for all DoFs is 512 per revolution of the motor, providing in combination with the gear ratios sufficient resolution at the link side for high accuracy motion. The robot is equipped with a *Nano43* 6 axis force/torque sensor from *ATI Industrial Automation*. The particular mounting is described in detail in Sect. 3. A sample rate of 670 Hz is used to realize the force control law presented in Sect. 4.

Table 1. Denavit-Hartenberg parameters.

	α_i	a_i	Θ_i	d_i		α_i	a_i	Θ_i	d_i
${}^0\boldsymbol{T}_1$	70°	0	Θ_1	0	${}^2\boldsymbol{T}_3$	-60°	0	Θ_3	0
${}^1\boldsymbol{T}_2$	-70°	0	Θ_2	0	${}^3\boldsymbol{T}_4$	0	0	0	$-d_4$

The modified Denavit-Hartenberg (DH) parameters as shown in Fig. 2 (together with the relevant frames) are summarized in Table 1. The overall transformation from the instrument tip frame F_4 to the robot base frame F_0 is:

$$ {}^0\boldsymbol{T}_4 = {}^0\boldsymbol{T}_1 {}^1\boldsymbol{T}_2 {}^2\boldsymbol{T}_3 {}^3\boldsymbol{T}_4 = \begin{bmatrix} {}^0\boldsymbol{R}_4^{3\times 3} & \boldsymbol{v} \\ \boldsymbol{0}^T & 1 \end{bmatrix} . \tag{1} $$

Noticing that the angle Θ_3 does not affect the instument tip position $\boldsymbol{v}$, one selects the following vector in order to parameterize the 4 instrument's DoFs:

$$ \boldsymbol{x} = [\boldsymbol{v}^T(\Theta_1, \Theta_2, d_4),\ \ \Theta_3]^T . \tag{2} $$

In the rest of the paper, the angle Θ_3 is considered to be fixed, and only the position $\boldsymbol{v}$ of the instrument tip is controlled. The Jacobian $\boldsymbol{J}^{3\times 3}$ for the translational DoFs can thus be written as:

$$ \boldsymbol{J} = \frac{\partial \boldsymbol{v}}{\partial \left[\Theta_1,\ \Theta_2,\ d_4\right]^T} . \tag{3} $$

The singularities of the translational workspace are given by the solutions of:

$$ \det(\boldsymbol{J}) = 0 = -\mathrm{d}_4^2 \sin(\alpha_1) \sin(\alpha_2) \sin(\Theta_2) . \tag{4} $$

Thus, singularities are encountered when:

$$ d_4 = 0 , \quad \text{or} \quad \Theta_2 = \pm \mathrm{k}\pi \quad \text{with} \quad \mathrm{k} = 0, 1, 2, ... \tag{5} $$

The first singularity, which is of second order, is reached when the instrument tip is at the fulcrum point. It has no consequence during experiments. Indeed, it is crossed only when inserting or removing the instrument, which can be done under joint position control. For the second singularity, $\Theta_2 = \pi$ cannot be reached due to joint limits. Thus, the only physically feasible singularity is $\Theta_2 = 0$, which separates the workspace into two parts. During in vivo experiments, one chooses initially for $\Theta_2 > 0$ or $\Theta_2 < 0$ and the singularity is never crossed.

3 Force Measurement

In manual MIS manipulation forces cannot be sensed by the surgeon anymore, due to the friction in the trocar. It is expected that force measurement and force feedback in MIRS increase the immersion of the surgeon into the remote side. Furthermore, measurement of forces is a prerequisite for force control. This, again, helps to avoid damage of tissue and suturing material and might also lead to new operation techniques as manipulation with predefined forces become possible [4,2,3].

Force measurement can be realized by placing miniaturized force/torque sensors near the instrument tip inside the patient [5]. Here, questions of sterilizability and electromagnetic compatibility still need to be answered. Alternatively, if the force sensor was integrated in the instrument shaft and placed outside the patient, disruption of the force measurement would occur due to friction in the trocar and torques necessary to rotate the trocar around the fulcrum point. This would be especially the case in heart surgery where the trocar is placed in the narrow space between the ribs.

3.1 Measurement Principle

The solution proposed here is a new trocar in which the sensor is integrated, but placed outside the patient, avoiding the before mentioned problems. This is possible, as the trocar is moved (and so is the force sensor) to realize motion inside the patient (see Sect. 2). The trocar is depicted in Fig. 3: the instrument is placed inside a passive guidance, which increases the rigidity of the system. The passive guidance is attached to the upper part of the force/torque sensor. The lower part of the sensor is placed on a conventional trocar. This set up allows for the measurement of the interaction forces between instrument tip and tissue, without having to cope with friction inside the trocar. The dynamic equation of the instrument (1) writes:

$$0 = \boldsymbol{w}_{2\to1} + \boldsymbol{w}_{3\to1} + \boldsymbol{w}_{7\to1} + \boldsymbol{w}_{g\to1} - \boldsymbol{w}_{d_1} \ , \tag{6}$$

where $\boldsymbol{w}_{i\to j}$ denotes the wrench applied by part i to part j, $\boldsymbol{w}_{g\to i}$ is the wrench applied to part i due to gravity, and $\boldsymbol{w}_{d_i}$ is the dynamic wrench of part i, accounting for the inertial effects due to acceleration. Similarily, the dynamic equations of parts (2) and (3) are:

$$0 = \boldsymbol{w}_{1\to2} + \boldsymbol{w}_{3\to2} + \boldsymbol{w}_{g\to2} - \boldsymbol{w}_{d_2} \ , \tag{7}$$

$$0 = \boldsymbol{w}_{2\to3} + \boldsymbol{w}_{1\to3} + \boldsymbol{w}_{4\to3} + \boldsymbol{w}_{g\to3} - \boldsymbol{w}_{d_3} \ . \tag{8}$$

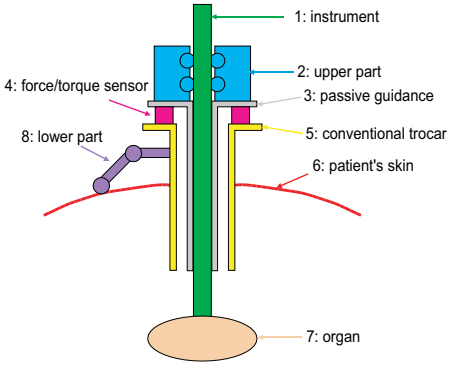

Fig. 3. Modified trocar with integrated force.

The wrench $\boldsymbol{w}_{1\to7} = -\boldsymbol{w}_{7\to1}$ is the interaction of interest (between instrument and organ) whereas $\boldsymbol{w}_{4\to3}$ is the wrench measured by the sensor. Summing Eq. 6, Eq. 7, and Eq. 8 yields:

$$\boldsymbol{w}_{1\to7} = \boldsymbol{w}_{4\to3} + \boldsymbol{w}_g - \boldsymbol{w}_d \,, \tag{9}$$

where $\boldsymbol{w}_g$ and $\boldsymbol{w}_d$ are the total gravity wrench and dynamic wrench, respectively:

$$\boldsymbol{w}_g = \boldsymbol{w}_{g\to1} + \boldsymbol{w}_{g\to2} + \boldsymbol{w}_{g\to3} \quad \text{and} \quad \boldsymbol{w}_{\mathrm{d}} = \boldsymbol{w}_{\mathrm{d}_1} + \boldsymbol{w}_{\mathrm{d}_2} + \boldsymbol{w}_{\mathrm{d}_3} \,. \tag{10}$$

Remarkably, neither the friction between the instrument and the passive guidance, $\boldsymbol{w}_{1\to3}$, nor the wrench between the trocar and the patient's skin, $\boldsymbol{w}_{5\to6}$, influence the measurement. Therefore, there is no need for any model of these disturbances. Rather, in order to calculate the interaction wrench $\boldsymbol{w}_{1\to7}$ one has to know the gravitation wrench $\boldsymbol{w}_g$ and the dynamic wrench $\boldsymbol{w}_d$. Usually, $\boldsymbol{w}_d \approx 0$ holds, as velocities and accelerations in MIS are rather small. Therefore, in practice, estimating the distal interaction $\boldsymbol{w}_{1\to7}$ from the measured wrench $\boldsymbol{w}_{4\to3}$ is reduced to a gravity compensation algorithm, which is detailed in the next section.

3.2 Gravity Compensation

The influence of gravity is calculated using a model of the robot whith several unknown parameters, which need to be identified. These parameters can be divided into two groups: fixed parameters which do not change between experiments and variable parameters which vary between experiments. The fixed parameters are calculated offline, only once, whereas the others need to be calculated online at the beginning of each experiment.

The fixed parameters are the angle ψ describing the rotation about the z_4-axis between the sensor frame $\mathcal{F}_s$ and frame $\mathcal{F}_3$, as well as the center of gravity ${}^sG$ (expressed in $\mathcal{F}_s$) of the parts 1, 2, and 3 of the robot, as depicted in Fig. 2 and Fig. 3.

One of the variable parameters is the unknown weight ${}^0\boldsymbol{p} = m\,{}^0\boldsymbol{g}$ expressed in the robot base frame $\mathcal{F}_0$. This parameter is variable since the robot is mounted on

the patient in an arbitrary orientation. Furthermore, the sensor measurement offsets (${}^s\boldsymbol{f}_o$ for forces and ${}^s\boldsymbol{t}_o$ for torques), and the mass m of the parts 1, 2, and 3 of the robot are not known. Note, that the mass m does not change during the experiments, but m can be easily estimated online, too:

$$m = \frac{\|{}^0\boldsymbol{p}\|_2}{9.81\ \mathrm{m/s^2}} \ . \tag{11}$$

Therefore, m can be used to verify the online calibration results. With these parameters the following model for forces due to gravity ${}^s\boldsymbol{f}_m$ can be defined (in sensor frame $\mathcal{F}_s$):

$${}^s\boldsymbol{f}_m = {}^s\boldsymbol{R}_3\,{}^3\boldsymbol{R}_0\,{}^0\boldsymbol{p} + {}^s\boldsymbol{f}_o \ . \tag{12}$$

For the torques the following equation holds (again in sensor frame $\mathcal{F}_s$):

$${}^s\boldsymbol{t}_m = \left[{}^s\boldsymbol{R}_3\,{}^3\boldsymbol{R}_0\,{}^0\boldsymbol{p}\right] \times {}^s\boldsymbol{d}_{GS} + {}^s\boldsymbol{t}_o = -[{}^s\boldsymbol{d}_{GS}]_\times \left[{}^s\boldsymbol{R}_3\,{}^3\boldsymbol{R}_0\,{}^0\boldsymbol{p}\right] + {}^s\boldsymbol{t}_o \ , \tag{13}$$

where ${}^s\boldsymbol{d}_{GS}$ is the vector from G to the center S of $\mathcal{F}_s$, expressed in $\mathcal{F}_s$, and $[\boldsymbol{a}]_\times$ denotes the skew symmetric matrix associated with a vector $\boldsymbol{a}$ such that, for any vector $\boldsymbol{b}$, $[\boldsymbol{a}]_\times \boldsymbol{b} = \boldsymbol{a} \times \boldsymbol{b}$. The vector ${}^0\boldsymbol{p}/\|{}^0\boldsymbol{p}\|_2$ represents the unknown orientation of the gravity vector in the robot base frame $\mathcal{F}_0$. For matrix ${}^3\boldsymbol{R}_0$ the following relation holds:

$${}^3\boldsymbol{R}_0(\Theta_1, \Theta_2) = ({}^0\boldsymbol{R}_3)^{-1} = ({}^0\boldsymbol{R}_1\,{}^1\boldsymbol{R}_2\,{}^2\boldsymbol{R}_3)^{-1} \ , \tag{14}$$

that can be computed from the geometric model of the robot. The matrix ${}^s\boldsymbol{R}_3(\psi) = \mathrm{rot}(\psi, \boldsymbol{z}_3)$ describes the rotation ψ about the z-axis between the sensor frame $\mathcal{F}_s$ and frame $\mathcal{F}_3$.

For the offline calibration $N = 100$ points covering the workspace were chosen and the joint values

$$\Theta_{1,i} \quad \text{and} \quad \Theta_{2,i} \quad \text{with} \quad i = 1, .., N \ . \tag{15}$$

are recorded. The sensor force values ${}^s\boldsymbol{f}_{s,i}$ and torque values ${}^s\boldsymbol{t}_{s,i}$ are simultaneously recorded. During this motion the instrument does not touch the environment, and the wrench is measured when the robot stays still ($i.e.\ \boldsymbol{w}_d = 0$), so that the transmission model (Eq. 9) reduces to:

$$0 = \boldsymbol{w}_{4\to3} + \boldsymbol{w}_g \ , \tag{16}$$

which means that the measure matches the gravity wrench.

For each position, the force ${}^s\boldsymbol{f}_{m,i}(\Theta_{1,i}, \Theta_{2,i}, {}^0\boldsymbol{p}, {}^s\boldsymbol{f}_o, \psi)$ is calculated according to Eq. 12. The optimal values for the unknown parameters are assumed to be at the minimum of the error function

$${}^s e_f = \frac{1}{N} \sum_{i=1}^{N} ({}^s\boldsymbol{f}_{m,i} - {}^s\boldsymbol{f}_{s,i})^T ({}^s\boldsymbol{f}_{m,i} - {}^s\boldsymbol{f}_{s,i}) \ . \tag{17}$$

Table 2. Optimization results for the angle ψ, the components of the gravitation forces ${}^0\boldsymbol{g}$ forces, and the force offset ${}^s\boldsymbol{f}_o$ of the sensor.

$\psi[rad]$	${}^0g_x$ [N/kg]	${}^0g_y$ [N/kg]	${}^0g_z$ [N/kg]	m [kg]	${}^sf_{o,x}$[N]	${}^sf_{o,y}$[N]	${}^sf_{o,z}$ [N]
$\approx 3\pi/2$	0.0	-0.66	-9.79	0.289	0.64	2.8	1.28

To calculate the unknown parameters a gradient based approach is used, as ${}^se_f$ is a nonlinear function of ψ. The optimization results are summarized in Table 2. In this experiment the robot was placed on an approximately horizontal table, thus the estimated gravity field vector ${}^0\boldsymbol{g} = {}^0\boldsymbol{p}/m$ is expected to be close to ${}^0\boldsymbol{g}_{\rm th} = [0, 0, -9.81\mathrm{N/kg}]^T$. The angle β between the calculated ${}^0\boldsymbol{g}$ and ${}^0\boldsymbol{g}_{\rm th}$ is $\beta = 3.87$ deg.

These results are now used to calculate the unknown offset ${}^s\boldsymbol{t}_o$ and the unknown center of gravity ${}^sG$. The following error function is used:

$$ {}^se_t = \frac{1}{N}\sum_{i=1}^{N}({}^s\boldsymbol{t}_{m,i} - {}^s\boldsymbol{t}_{s,i})^T({}^s\boldsymbol{t}_{m,i} - {}^s\boldsymbol{t}_{s,i}) \; . \tag{18} $$

The results are summarized in Table 3 (note, the point ${}^sG$ is expressed in frame F_s).

Table 3. Optimization results for the center of gravity ${}^s\boldsymbol{G}$ and the torque offset ${}^s\boldsymbol{t}_o$ of the sensor.

${}^sG_x$ [mm]	${}^sG_y$ [mm]	${}^sG_z$ [mm]	${}^st_{o,x}$ [Nmm]	${}^st_{o,y}$ [Nmm]	${}^st_{o,z}$ [Nmm]
1.44	-4.42	42.2	-111	21.1	4.1

The high accuracy of this approach can be seen in Fig. 4 where the measured data and the model based (calculated) values are given.

4 Force Control

This section describes the chosen force control structure in detail and gives first experimental results.

At the lowest level of the controller, a joint position loop encapsulates the joint velocity loop realized in hardware by the power amplifiers. This joint position loop uses a simple proportional gain, avoiding the use of an integral term. As a consequence, the joint position servo loop is not extremely precise, but keeps enough bandwidth available for the outer force feedback loop.

The force feedback loop computes a velocity, fed to the position controller through an integrator. Although, a desired force ${}^4\boldsymbol{f}_d = [{}^4f_{d,x}, {}^4f_{d,y}, {}^4f_{d,z}]^T$ is to be exerted by the instrument tip on the organ, the vector ${}^4\boldsymbol{h} = [{}^4t_y, {}^4t_x, {}^4f_z]^T$ was chosen in order to be servoed. The vector ${}^4\boldsymbol{h}$ is constituted by the two components of the torque at the fulcrum point O that belong the plane $(O, \boldsymbol{x}_4, \boldsymbol{y}_4)$ and the force component along the instrument penetration axis $(O, \boldsymbol{z}_4)$.

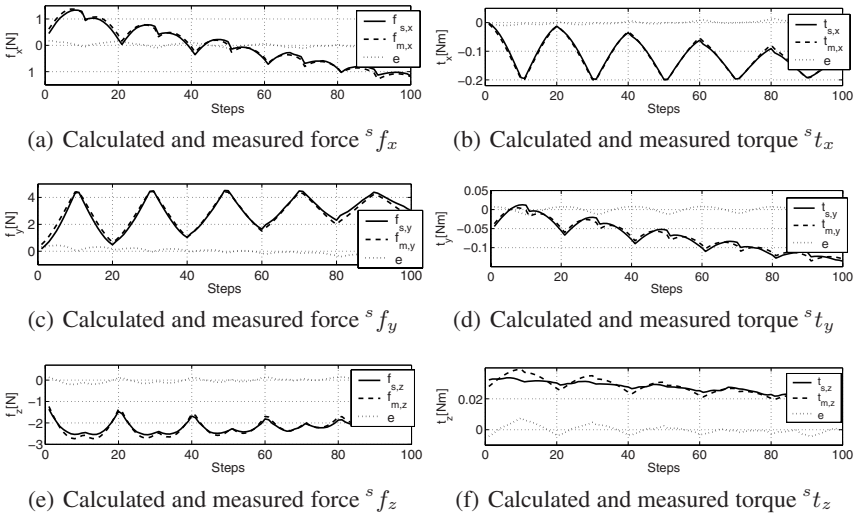

(a) Calculated and measured force ${}^{s}f_x$ (b) Calculated and measured torque ${}^{s}t_x$

(c) Calculated and measured force ${}^{s}f_y$ (d) Calculated and measured torque ${}^{s}t_y$

(e) Calculated and measured force ${}^{s}f_z$ (f) Calculated and measured torque ${}^{s}t_z$

Fig. 4. Calculated and measured forces and torques in F_s during the offline calibration procedure. Furthermore, the error e is given.

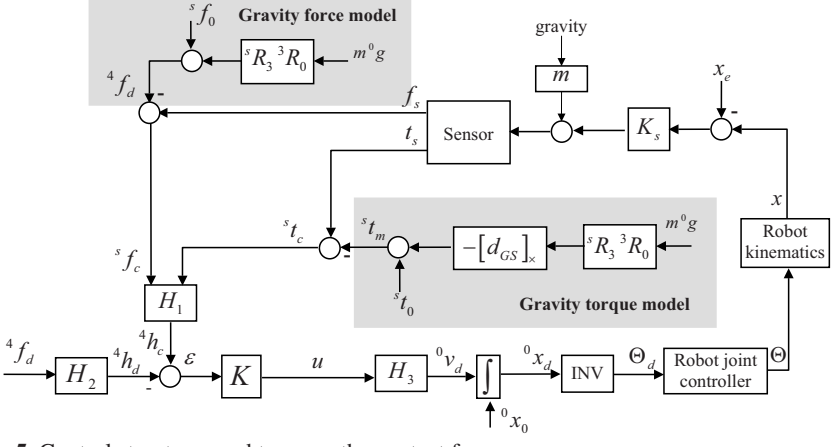

Fig. 5. Control structure used to servo the contact forces.

This vector was chosen in order to provide a stable behavior when operating in a comanipulation mode: in this case, the system runs a transparency mode, *i.e.* a force controlled mode with a zero desired value. Therefore, when a force is applied to the instrument, the robot must produce a motion that attempts to cancel the force. Moreover, the system should be transparent for forces exterted either by an organ inside a patient, or by the surgeon outside the patient. This situation is sketched in Fig. 6, for a simplified planar case of an instrument constrained by a fulcrum point.

In order to cancel out the external forces (red arrows in Fig. 6) the velocity which has to be provided by the controller has two components (blue arrows in Fig. 6):

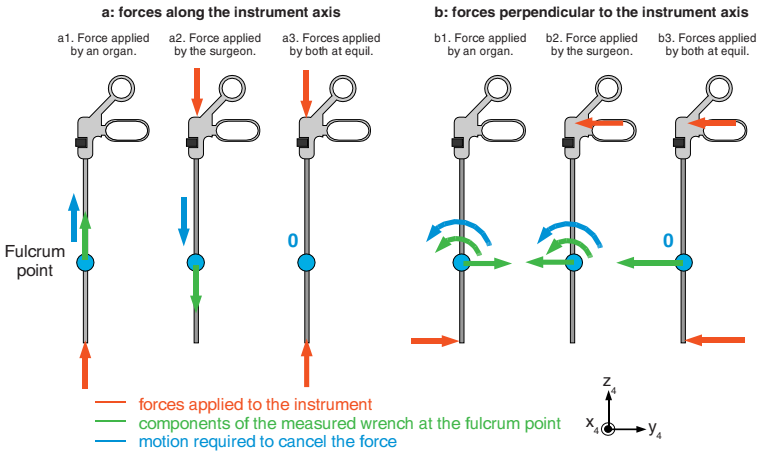

Fig. 6. Forces, torques, and motions involved during co-manipulation.

the linear velocity ${}^4v_z$ along $\boldsymbol{z}_4$ (case shown in Fig. 6 a) and rotational velocity ${}^4\omega_x$ along $\boldsymbol{x}_4$ (case shown in Fig. 6 b). Additionally, the measured forces (two planar components ${}^4f_y$ and ${}^4f_z$) and torque at the fulcrum point (one component ${}^4t_x$) corresponding to the externally applied force are represented in green. Note that, in this example the wrench is measured at the fulcrum point, whereas for MC^2E this is not the case. Furthermore, the influence of the instrument weight on the measurements is neglected here (as they are compensated for in the experiments).

One can see in Fig. 6 a1 and Fig. 6 a2 that the velocity ${}^4v_z$ is always in the direction of the measured force ${}^4f_z$. Therefore, a simple proportional control law:

$$ {}^4v_z = k\ {}^4f_z \tag{19}$$

is appropriate for both cases. On the contrary, in Fig. 6 b1, the measured force ${}^4f_y$ and the cancelling velocity ${}^4\omega_x$ are both positive, while in Fig. 6 b2, they have an opposite sign. Therefore, selecting the force ${}^4f_y$ as a component to be servoed is not appropriate for the control of ${}^4\omega_x$: a positive (resp. negative) gain would lead to unstable behavior with respect to outer (resp. inner) forces. That is why the following control was selected:

$$ {}^4\omega_x = k\ {}^4t_x\ . \tag{20}$$

Indeed, ${}^4\omega_x$ and ${}^4t_x$ have the same sign (positive) in both Fig. 6 b1 and Fig. 6 b2. Finally, note that in comanipulation, when there is an equilibrium between the surgeon force and the organ force, the system stays still (see Fig. 6 a3 and Fig. 6 b3). This allows for the surgeon to feel the distal forces from the proximal grasp. Generalizing this reasonning to the 3 DoFs problem, the final control law for a zero desired force consists of computing the velocity command vector $\boldsymbol{u}$:

$$ \boldsymbol{u} = \begin{bmatrix} {}^4\omega_x \\ {}^4\omega_y \\ {}^4v_z \end{bmatrix} = \boldsymbol{K} \begin{bmatrix} {}^4t_x \\ {}^4t_y \\ {}^4f_z \end{bmatrix}\ , \tag{21}$$

where $\boldsymbol{K}$ is a diagonal matrix of positive gains.

In order to apply this control law to MC^2E the wrench measured by the sensor $({}^s\boldsymbol{f}_s, {}^s\boldsymbol{t}_s)$ given in frame $\mathcal{F}_s$ at point S has to be gravity compensated, which gives the contact situation (*i.e.* the external wrench)

$$\begin{bmatrix} {}^s\boldsymbol{f}_c \\ {}^s\boldsymbol{t}_c \end{bmatrix} = \begin{bmatrix} {}^s\boldsymbol{f}_s \\ {}^s\boldsymbol{t}_s \end{bmatrix} - \begin{bmatrix} {}^s\boldsymbol{f}_m \\ {}^s\boldsymbol{t}_m \end{bmatrix} , \tag{22}$$

and then transformed in the frame $(O, \boldsymbol{x}_4, \boldsymbol{y}_4, \boldsymbol{z}_4)$ located at the fulcrum point O:

$${}^4\boldsymbol{h}_c = \begin{bmatrix} {}^4t_x \\ {}^4t_y \\ {}^4f_z \end{bmatrix} = \boldsymbol{H}_1 \begin{bmatrix} {}^s\boldsymbol{f}_c \\ {}^s\boldsymbol{t}_c \end{bmatrix} , \tag{23}$$

$({}^s\boldsymbol{f}_m, {}^s\boldsymbol{t}_m)$ being the model based gravity compensation and the transformation matrix

$$\boldsymbol{H}_1 = \begin{bmatrix} 000100 \\ 000010 \\ 001000 \end{bmatrix} \begin{bmatrix} {}^4\boldsymbol{R}_s & \boldsymbol{0}^{3\times3} \\ {}^4\boldsymbol{R}_s[\boldsymbol{d}_{SO}]_\times & {}^4\boldsymbol{R}_s \end{bmatrix} . \tag{24}$$

In order to be able to specify a desired force ${}^4\boldsymbol{f}_d = [{}^4f_{d,x}, {}^4f_{d,y}, {}^4f_{d,z}]^T$ at the instrument tip P, one needs to compute the corresponding desired components for the servoed vector ${}^4\boldsymbol{h}_d$:

$${}^4\boldsymbol{h}_d = \begin{bmatrix} {}^4t_{d,x} \\ {}^4t_{d,y} \\ {}^4f_{d,z} \end{bmatrix} = \begin{bmatrix} 0 & -d_4 & 0 \\ d_4 & 0 & 0 \\ 0 & 0 & 1 \end{bmatrix} \begin{bmatrix} {}^4f_{d,x} \\ {}^4f_{d,y} \\ {}^4f_{d,z} \end{bmatrix} = \boldsymbol{H}_2 \begin{bmatrix} {}^4f_{d,x} \\ {}^4f_{d,y} \\ {}^4f_{d,z} \end{bmatrix} . \tag{25}$$

The final control law, accounting for the desired force vector is:

$$\boldsymbol{u} = \boldsymbol{K} \left(\boldsymbol{H}_1 \begin{bmatrix} {}^s\boldsymbol{f}_c \\ {}^s\boldsymbol{t}_c \end{bmatrix} - \boldsymbol{H}_2 \begin{bmatrix} {}^4f_{d,x} \\ {}^4f_{d,y} \\ {}^4f_{d,z} \end{bmatrix} \right) . \tag{26}$$

Thereafter, the command vector $\boldsymbol{u}$ is converted into the desired instrument tip velocity ${}^0\boldsymbol{v}_d$, expressed in the robot base frame $\mathcal{F}_0$ by

$${}^0\boldsymbol{v}_d = {}^0\boldsymbol{R}_4 \boldsymbol{H}_2^T \boldsymbol{u} = \boldsymbol{H}_3 \boldsymbol{u} \tag{27}$$

and then integrated to the desired position ${}^0\boldsymbol{x}_d$. An iterative inverse model is used to compute the desired joints $\boldsymbol{\Theta}_d$ of the robot which are passed to the robot joint controller. As the robot moves, the instrument touches the environment (here modeled as spring $\boldsymbol{K}_s$) located at $\boldsymbol{x}_e$.

Experimental results are given in Fig. 7 for ${}^4f_{c,x}$, ${}^4f_{c,y}$, and ${}^4f_{c,z}$. It can be seen that the desired contact forces are achieved, whithout a remaining offset. Nevertheless, a significant rise time occurs, mainly due to the soft environment used as a subsitute for real organs.

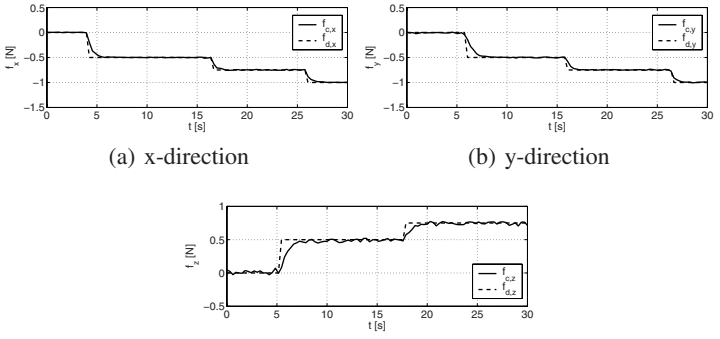

(a) x-direction (b) y-direction

(c) z-direction

Fig. 7. Trajectories of the desired (${}^4f_d$) and measured (${}^4f_c$) contact force in tool tip frame $\mathcal{F}_4$.

5 Conclusions and Outlook

In this paper a compact and lightweight robot for force control in MIS is presented. This robot posesses an invariant point due to its kinematics and is mounted on the patient. A new trocar with an integrated force sensor allowing for the measurement of contact forces is described. Although this sensor is placed outside the patient friction inside the trocar does not deteriorate the measurements. Experimental force control results are given, validating the chosen concepts. Future work includes the setup of a force reflecting telemanipulation system for MIS, which will provide a realistic impression of the remote forces to the surgeon.

References

1. Russell H. Taylor and Dan Stoianovici. Medical robotics in compter-integrated surgery. *IEEE Transactions on Robotics and Automation*, 19(5):765–781, 2003.
2. C. Wagner, N. Stylopoulos, and R. Howe. The role of force feedback in surgery: Analysis of blunt dissection. In *Proc. of the 10th Annual Haptics Symposium*, March 2002.
3. B. Deml, T. Ortmaier, and H. Weiss. Minimally invasive surgery: Empirical comparison of manual and robot assisted force feedback surgery. In *Proceedings of the 4th International Conference EuroHaptics 2004*, Munich, Germany, June 2004.
4. T. Ortmaier. *Motion Compensation in Minimally Invasive Robotic Surgery*. VDI Verlag, 2003. PhD Thesis.
5. U. Seibold and G. Hirzinger. A 6-axis force/torque sensor design for haptic feedback in minimally invasive robotic surgery. In *Proceedings of the 2nd VDE World Microtechnologies Congress*, Munich, Germany, October 2003.
6. P. Berkelman, E. Boidard, P. Cinquin, and J. Troccaz. LER: The light endoscope robot. In *Proc. of the IEEE/RSJ International Conference on Intelligent Robots and Systems IROS 2003*, Las Vegas, USA, October 2003.
7. Yuki Kobayashi, Shingo Chiyoda, Kouichi Watabe, Masafumi Okada, and Yoshihiko Nakamura. Small occupancy robotic mechanisms for endoscopic surgery. In *Medical Image Computing and Computer-Assisted Intervention - MICCAI 2002: 5th International Conference, Proceedings, Part 1*, Tokyo, Japan, September 2002.